INTERNATIONAL JOURNAL FOR NUMERICAL METHODS IN FLUIDS
Int. J. Numer. Meth. Fluids 2004; **44**:579–597 (DOI: 10.1002/fld.659)

A novel method for automated grid generation of ice shapes for local-flow analysis

Egemen Ogretim[†] and Wade W. Huebsch[*,‡,§]

Mechanical and Aerospace Engineering Department, West Virginia University, Morgantown, WV, U.S.A.

SUMMARY

Modelling a complex geometry, such as ice roughness, plays a key role for the computational flow analysis over rough surfaces. This paper presents two enhancement ideas in modelling roughness geometry for local flow analysis over an aerodynamic surface. The first enhancement is use of the leading-edge region of an airfoil as a perturbation to the parabola surface. The reasons for using a parabola as the base geometry are: it resembles the airfoil leading edge in the vicinity of its apex and it allows the use of a lower apparent Reynolds number. The second enhancement makes use of the Fourier analysis for modelling complex ice roughness on the leading edge of airfoils. This method of modelling provides an analytical expression, which describes the roughness geometry and the corresponding derivatives. The factors affecting the performance of the Fourier analysis were also investigated. It was shown that the number of sine–cosine terms and the number of control points are of importance. Finally, these enhancements are incorporated into an automated grid generation method over the airfoil ice accretion surface. The validations for both enhancements demonstrate that they can improve the current capability of grid generation and computational flow field analysis around airfoils with ice roughness.

KEY WORDS: CFD; aircraft icing; stream function–vorticity; Prandtl transposition; Fourier; grid generation

1. INTRODUCTION

Surface geometry modelling for the flow field analysis over rough surfaces is an important task in CFD studies. Abrupt changes in the surface geometry of the roughness can make it difficult to generate a quality grid. Also, the convex parts of the roughness geometry may cause the grid cells to overlap at points away from the surface. Even with a commercial grid generation package and a moderate two-dimensional ice shape, it can take extensive man-hours to create a useable grid for flow analysis. This is why grid generation for the rough

*Correspondence to: W. W. Huebsch, Mechanical and Aerospace Engineering Department, West Virginia University, P.O. Box 6106, Morgantown, WV 26506-6106, U.S.A.
[†]Graduate Research Assistant
[‡]E-mail: wade.huebsch@mail.wvu.edu
[§]Assistant Professor.

Received 9 April 2003
Revised 15 September 2003

surfaces is still a challenging and time consuming process, particularly for ice roughness on a wing.

LEWICE and SMAGGICE, which are explained in detail in References [1, 2], respectively, are commonly used software tools for the numerical flow field analysis of airfoils with ice roughness, as in the study by Cebeci and Besnard [3]. The baseline LEWICE employs a panel method for the flow solver. However, a grid-generator and Navier–Stokes flow solver can be used with LEWICE in order to better capture the flow physics and make a more accurate ice accretion prediction. SMAGGICE is a semi-automatic, specialized grid generation package that is used to generate a structured grid around iced airfoils. The way that these algorithms deal with the difficulties of grid generation for ice roughness is to create blocks over the roughness geometry where necessary, and to use very fine grid resolution in order to decrease the effect of violation of orthogonality. This is a common practice for other algorithms that employ a structured grid scheme. The benefit of this practice is that the flow field in the convex areas of the roughness geometry is covered by these extra blocks and the problem of having overlapping grid cells is minimized.

The methods of creating extra blocks and/or refining the grid are techniques not unique to those researchers who are using LEWICE or SMAGGICE. Chung *et al.* [4] and Chung and Addy [5] used one fine-grid inner block and one outer block to overcome orthogonality difficulties. Chi *et al.* [6] employed several blocks to cover the flow field neighboring the roughness in order to avoid orthogonality and overlapping grid cell problems.

Thompson and Soni [7] also used a structured grid approach but the way they overcame some of the grid generation problems for ice roughness is different than the other two solutions mentioned above. They used a weighting function, which adjusts the skewness of the grid lines automatically. The other typical method employed for flow field analysis over rough surfaces is an unstructured grid. Dunn and Loth [8] used an unstructured grid to study the effects of simulated spanwise ice shapes. It should be noted that, to date, there is no clear advantage on the use of unstructured grids for wing icing problems.

One other group of studies on flow field analysis on rough surfaces focuses on a parabola as their base geometry, since it resembles many 4 digit airfoils in the leading-edge region and there is an analytical solution for the potential flow past a parabola [9], which is taken advantage of in this work. Another benefit of using this type of approach is that it enables the governing flow equations to use a lower Reynolds number (based on leading-edge radius of curvature), while the results can still be transformed to actual flight Reynolds numbers. In addition, it enables the algorithm to focus the computational resources in a small region (i.e. the leading-edge) so that a more detailed flow field analysis is possible. There is one further benefit, which can be realized through the use of a Prandtl transposition, or shearing transformation, in conjunction with the parabola. The roughness present on the airfoil surface, and hence the parabola surface, can be suppressed by embedding it in the governing equations through the Prandtl transposition. As a result of this suppression, the base geometry over which the grid generation is applied becomes a smooth surface, which in turn eases the grid generation process.

This study is a continuation of the work done by Huebsch and Rothmayer [9] in which unsteady viscous flow was simulated for flow past a parabola with analytic roughness shapes. The first enhancement in this study is the implementation of the leading edge of the actual airfoil as a ‘negative’ perturbation to the parabola baseline. The geometric similarity between the parabola and the leading edge of the NACA 0012 airfoil can be seen in Figure 1. The

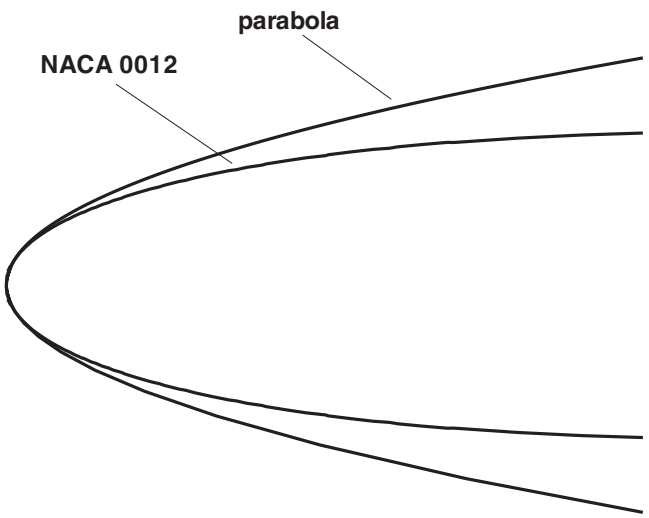

Figure 1. Leading-edge region of the airfoil and the parabola.

parabola leading edge matches the airfoil geometry up to approximately six percent of airfoil chord. But downstream of that location, the airfoil deviates from the parabola surface significantly. Therefore implementing the actual airfoil geometry as a perturbation to the parabola baseline surface is necessary both for more realistic results at downstream points as well as improving the accuracy of the simulations and the comparisons for the unsteady flow in the leading-edge region.

The second enhancement is a novel approach for modelling roughness on the leading edge of the airfoil. It is well known that by means of the Fourier analysis, a complex signal may be decomposed into its components and therefore can be expressed by a function of sine and cosine terms. The Fourier analysis was selected as the tool for roughness shape analysis because many roughness geometries, in particular ice roughness, resemble the shape of a complex signal, which can be expressed in terms of sines and cosines. Applying the Fourier analysis to the roughness geometry enables us to obtain an analytic expression for the roughness shape as well as its required derivatives.

The rationale behind trying to describe an ice shape with a single analytic expression is a result of employing the Prandtl transposition to describe the roughness as a perturbation to the baseline geometry and avoiding discontinuity problems at the surface. The benefit of using the Prandtl transposition is that the roughness geometry, which was originally a positive perturbation on the parabola, is suppressed in terms of the flow solver and becomes embedded in the governing flow equations (see next section for description). As a result of this, the parabola remains as the base geometry. It is obvious that the grid generation over a clean parabola is less complicated than that over a parabola with a roughness. However, since the roughness geometry becomes embedded in the governing equations, it is more efficient to express the perturbation analytically. The use of a single analytic equation to describe the roughness also helps to alleviate curvature discontinuity problems that would appear at juncture points if other geometric fitting methods were used (e.g. splines).

Figure 2. NACA 0012 and the selected ice shape (I-1998-000092).

The method described in this paper is being developed with the idea of using experimental ice tracing shapes for the leading-edge roughness geometry as acquired from icing wind tunnels. Resulting ice geometries are available from the NASA Glenn Icing Branch. Several steps are required prior to applying the Fourier analysis to describe the ice shape. Initially, the ice shape is smoothed using the SMAGGICE software. The amount of smoothing applied was 50% in accordance with previous work [4]. The remaining steps involve scaling and transformation of the ice shape to generate the necessary perturbations to the baseline parabola surface, which are covered in the following section.

2. GOVERNING EQUATIONS

The governing flow equations are the stream function–vorticity version of the 2-D incompressible, unsteady Navier–Stokes equations, which are shown in non-dimensional form.

$$\omega_t + \psi_y \omega_x - \psi_x \omega_y = Re^{-1}(\omega_{xx} + \omega_{yy}) \tag{1}$$

$$\psi_{xx} + \psi_{yy} = -\omega \tag{2}$$

A series of transformations are applied to the governing equations to move from physical space to computational space, which are discussed below.

An experimental ice shape was chosen for this work along with the corresponding airfoil, which is shown in Figure 2. The ice shape and leading-edge geometry of the airfoil are first non-dimensionalized by the chord length, then scaled by the airfoil leading-edge radius to fit the parabola space. As a result of this scaling, the ice roughness and the airfoil leading edge can be seen as perturbations to the baseline parabola surface (Figure 3).

The gap between the original parabola surface and the airfoil surface becomes larger further downstream. Considering the downstream boundary conditions of the flow solver, it is advantageous to transition the airfoil leading-edge geometry back to the original parabola geometry [9]. Therefore a transition curve is added aft of the airfoil leading edge in order to ensure a smooth passage back to the main parabola surface. This transition curve is also a parabola which is created based on: the co-ordinates of the last airfoil point used, the surface derivative at this same point, and the co-ordinates of the junction point where the transition parabola meets the main parabola. The final version of the surface geometry in the physical plane is shown in Figure 4. A majority of the computational resources are focused on the leading-edge region and ice shape.

After scaling the airfoil and ice shape to parabola space, a conformal mapping is applied to map the physical x–y plane to the ξ'–η' plane, with the following equations:

$$x = \frac{\xi'^2 - \eta'^2}{2}, \quad y = \xi'\eta' \tag{3}$$

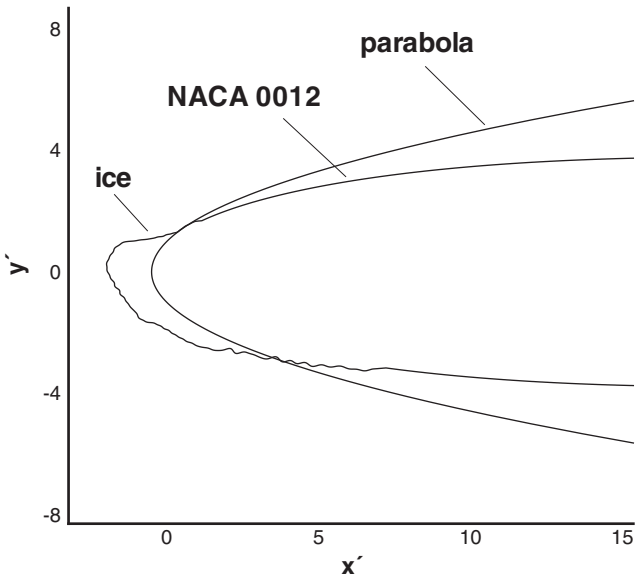

Figure 3. Ice shape transformed to the leading edge of the parabola.

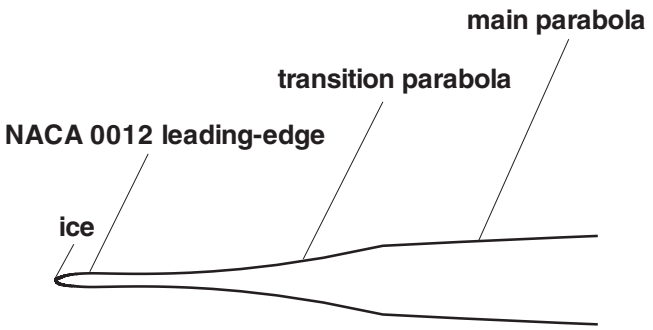

Figure 4. Overall geometry: ice shape, NACA0012, transition curve and the parabola.

With this mapping, the parabola surface in the physical plane becomes a line, where $\eta' = 1$ in the transformed ($\xi' - \eta'$) plane. The roughness geometry and leading-edge region of the airfoil, which were perturbations on the parabola, become perturbations to this line (see Figure 5).

Following the transformation to the ξ'–η' plane, the Prandtl transposition is applied to transform the variables to $\xi - \eta$ space through the following formulae:

$$\xi' = \xi, \quad \eta' = \eta + f(\xi) \tag{4}$$

where $f(\xi)$ is an analytic expression representing all of the perturbations on the $\eta' = 1$ line, including the roughness geometry. The only stipulation on the perturbation geometry for this transformation and for the Fourier analysis (discussed below) is that it has to be a single-

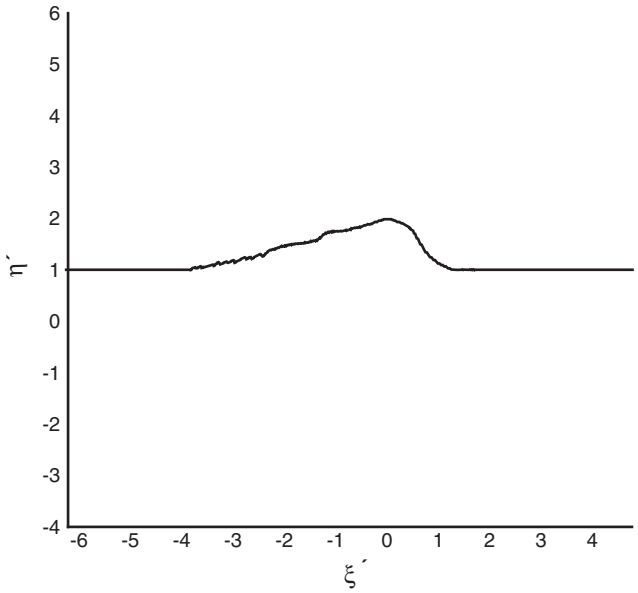

Figure 5. Parabola and the roughness in the transformed plane.

valued function in the ξ'–η' plane. For a majority of experimental ice shapes, this does not pose a problem with respect to the parabolic coordinate system. As a result of the Prandtl transposition, the perturbations off the straight line of $\eta' = 1$ originating from the ice roughness and the airfoil geometry are suppressed and the final surface geometry is a straight line in the ξ–η plane at $\eta = 1$.

The transformations outlined above are applied to the governing equations (Equations (1) and (2)). In addition, a technique of splitting the stream function and vorticity terms into a viscous and inviscid part is employed to improve convergence of the algorithm [10]. A final transformation to computational space, $\bar{\xi}$–$\bar{\eta}$, is applied that incorporates stretching and clustering of grid lines [9]. The transformations produce a uniform rectangular grid in $\bar{\xi}$–$\bar{\eta}$ space. The final stream function–vorticity transport equations are given as

$$\begin{aligned}
&\bar{\xi}_{\xi\xi}\Psi_{\bar{\xi}} + (\bar{\xi}_{\xi})^2\Psi_{\bar{\xi}\bar{\xi}} - f_{\xi\xi}\bar{\eta}_{\eta}\Psi_{\bar{\eta}} \\
&\quad - 2f_{\xi}\bar{\xi}_{\xi}\bar{\eta}_{\eta}\Psi_{\bar{\xi}\bar{\eta}} + (1 + (f_{\xi})^2)\bar{\eta}_{\eta\eta}\Psi_{\bar{\eta}} \\
&\quad + (1 + (f_{\xi})^2)(\bar{\eta}_{\eta})^2\Psi_{\bar{\eta}\bar{\eta}} = (-h^2)\Omega + \Psi_{\tau}
\end{aligned} \tag{5}$$

$$\begin{aligned}
&\Omega_{\tau} + h^2\Omega_t + \bar{\xi}_{\xi}\bar{\eta}_{\eta}(\Psi_{\bar{\eta}}\Omega_{\bar{\xi}} - \Psi_{\bar{\xi}}\Omega_{\bar{\eta}}) + (\psi_{\mathrm{inv}})_{\eta'}\bar{\xi}_{\xi}\Omega_{\bar{\xi}} - f_{\xi}(\psi_{\mathrm{inv}})_{\eta'}\bar{\eta}_{\eta}\Omega_{\bar{\eta}} \\
&\quad - (\psi_{\mathrm{inv}})_{\xi'}\bar{\eta}_{\eta}\Omega_{\bar{\eta}} = Re^{-1}[\bar{\xi}_{\xi\xi}\Omega_{\bar{\xi}} + (\bar{\xi}_{\xi})^2\Omega_{\bar{\xi}\bar{\xi}} - f_{\xi\xi}\bar{\eta}_{\eta}\Omega_{\bar{\eta}} - 2f_{\xi}\bar{\xi}_{\xi}\bar{\eta}_{\eta}\Omega_{\bar{\xi}\bar{\eta}} \\
&\quad + (1 + (f_{\xi})^2)\bar{\eta}_{\eta\eta}\Omega_{\bar{\eta}} + (1 + (f_{\xi})^2)(\bar{\eta}_{\eta})^2\Omega_{\bar{\eta}\bar{\eta}}]
\end{aligned} \tag{6}$$

The h^2 term is a scale factor equal to $\xi^2+\eta^2+2\eta f+f^2$. To help stabilize the algorithm during global iterations, a fictitious time-derivative term (or pseudo-time) is added to both the stream function and vorticity transport equations: Ψ_τ and Ω_τ, respectively. The inviscid solution for flow past a parabola with surface roughness present can be found from

$$\psi_{\text{inv}}=(\xi+K)(\eta+f-1) \tag{7}$$

The K term is the displacement of the stagnation point from the vertex of the parabola and can be related to the angle-of-attack of the airfoil. A more detailed discussion of these governing equations is provided in Huebsch and Rothmayer [9].

No-slip boundary conditions, with $u=v=0$, are applied at the surface. In terms of the stream function, and making use of the split variables, the no-slip boundary condition can be written as

$$\Psi=-\psi_{\text{inv}} \quad \text{and} \quad \Psi_{\bar{\eta}}=-\frac{(\psi_{\text{inv}})_\eta}{\bar{\eta}_\eta} \tag{8}$$

At the far-field boundary, η large but finite, the viscous effects die out and a fully inviscid flow is recovered. Therefore, the split viscous variables, Ψ and Ω, are set to zero at this boundary. At the far-downstream boundary, the flow is assumed to be steady, with the upper and lower downstream boundaries placed at a large, but finite value of $|\xi|$. Davis [11] has shown that the viscous solution for flow past a parabola approaches the Blasius solution as $\xi\to\infty$. The reader is referred to References [11, 9] for more details.

The impact of the Prandtl transposition can be clearly seen as the roughness perturbations on the base geometry become embedded in the governing equations. The f, $f_\xi, f_{\xi\xi}$ terms in these equations express the perturbation geometry, slope, and curvature on the parabola. With this final version of the governing equations, the perturbations are suppressed and the grid generation process is simplified. However, the perturbation geometry has to be expressed analytically to avoid jump discontinuity problems.

For the cases in which complex roughness shapes are involved (i.e. ice roughness) the Fourier analysis is used to obtain the analytical expression of the roughness geometry. The Fourier analysis requires the original roughness geometry data as well as the transformed version into the ξ'–η' plane. After this is completed, the following equations are used in order to obtain the analytical expression for the roughness shape:

$$a_i=\frac{2}{(\xi_N-\xi_1)}\int_{\xi_1}^{\xi_N} f(\xi)\cos\left(\frac{2\pi i\xi}{(\xi_N-\xi_1)}\right)\mathrm{d}\xi \quad i=0,1,2,\ldots \tag{9}$$

$$b_i=\frac{2}{(\xi_N-\xi_1)}\int_{\xi_1}^{\xi_N} f(\xi)\sin\left(\frac{2\pi i\xi}{(\xi_N-\xi_1)}\right)\mathrm{d}\xi \quad i=1,2,3,\ldots \tag{10}$$

$$\tilde{f}(\xi)=\frac{1}{2}a_0+\sum_{i=1}^{i=N}\left[\begin{array}{l} a_i\cos\left(\dfrac{2\pi i\xi}{(\xi_N-\xi_i)}\right) \\ +b_i\sin\left(\dfrac{2\pi i\xi}{(\xi_N-\xi_i)}\right)\end{array}\right] \tag{11}$$

where ξ_1 and ξ_N are the first and the last points, respectively, a_i's are the coefficients of the cosine terms, b_i's are the coefficients of the sine terms, $f(\xi)$ is the transformed roughness data and $\tilde{f}(\xi)$ is the analytic roughness expression in terms of the sine and cosine functions.

The flow simulations executed in this study made use of the full unsteady Navier–Stokes equations, but with a two-dimensional constraint. Appropriate spatial and temporal resolutions were implemented to resolve the geometry as well as capture the relevant flow physics. The flow solver is clean and robust with no requirement for explicit artificial dissipation or other dissipation inducing numerical devices. A detailed discussion of the algorithm is given in Reference [9].

An implicit numerical method is used to solve the governing flow equations, which is second-order accurate in time and space. One complete spatial sweep consists of two alternating sweeps in the streamwise direction and one sweep in the normal direction, which is equivalent to one pseudo time step. The algorithm is capable of solving for steady or unsteady flow. If the flow is unsteady, the code marches the solution in time and at each physical time step, the pseudo time terms are iterated to convergence before moving to the next physical time step. As a starting solution for the full Navier–Stokes calculations, the parabolized Navier–Stokes equations are solved for flow past a clean parabola at a constant angle-of-attack and the solution is used as input for the full Navier–Stokes. The parabolized Navier–Stokes solver uses the Blasius solution as a starting solution.

3. RESULTS AND DISCUSSION

The current study focuses on implementing new techniques for surface modelling on airfoils, with the goal of a more automated grid generation process when complex surface roughness is present. A local-flow Navier–Stokes algorithm is used to solve for the flow field in the leading-edge region of the airfoil and not have to include the entire airfoil. This allows the solver to place a dense grid in the region of interest. An example of the grid used over a single hump and its close-up are shown in Figures 6 and 7, respectively. Though the grid shown in Figure 7 is non-orthogonal in the surface perturbation region, the flow solver does not show any sensitivity to grid skewness. As discussed in the previous section, the grid around the parabola with perturbations is transformed to a uniform rectangular grid in computational space.

For verifying the newly implemented features for the surface geometry analysis (i.e. leading-edge of an airfoil and the Fourier analysis for roughness), various test cases were performed. First, use of the NACA 0012 leading-edge region as a perturbation to the parabola surface for modelling the airfoil geometry was tested. In the study by Huebsch and Rothmayer [9], the parabola was used to model the leading edge of a symmetric airfoil. But in the present study, the actual airfoil leading-edge surface is implemented as a perturbation to the parabola surface by means of the analytic formula for the NACA 0012. This allows a geometrical match further downstream than the 6% of chord limit of the parabola. The formula for the airfoil is given below in the ξ–η plane.

$$f = \frac{0.6}{0.0159\xi}(a\beta^{0.5} - b\beta - c\beta^2 + d\beta^3 - e\beta^4) - 1 \tag{12}$$

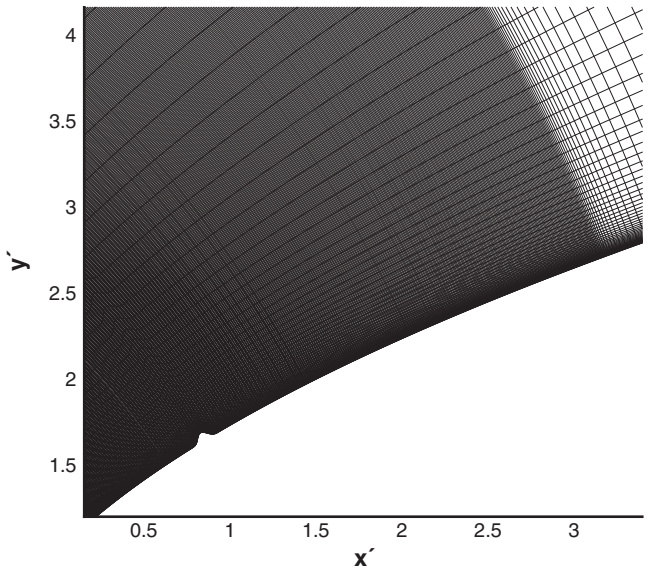

Figure 6. Overview of the mesh over parabola with a single hump.

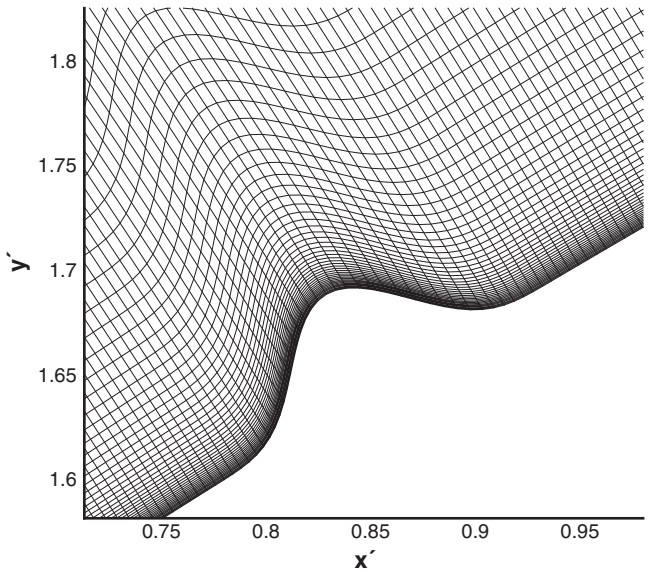

Figure 7. A close up of the mesh around the single hump.

where

$$a = 0.2969 \quad b = 0.1260 \quad c = 0.3510$$

$$d = 0.2843 \quad e = 0.1015 \quad \beta = \frac{0.0159}{2}(\xi^2 - 2f - f'^2)$$

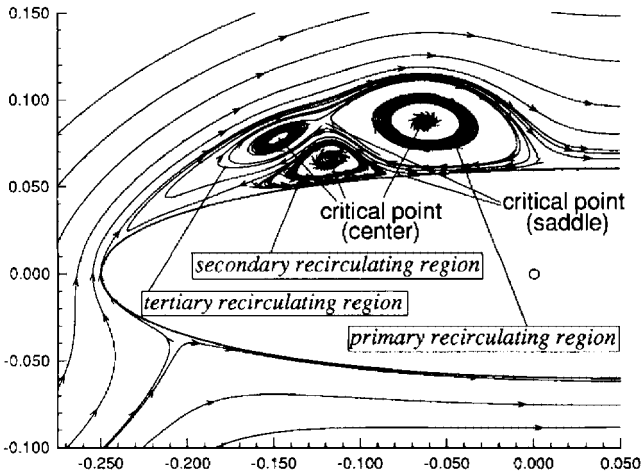

Figure 8. Contours over NACA 0012 in pitchup for the benchmark case.

Since the above equation for the f values defining the NACA 0012 airfoil is an implicit one, iteration methods are needed for obtaining these f values for the corresponding ξ values. In the course of the study it was seen that different iteration methods could result in an accurate solution for the f values. However the results may not be in good match for the f_ξ, and the $f_{\xi\xi}$ values, which are also defined by implicit analytic expressions. One would expect f_ξ to be symmetric with respect to the origin and $f_{\xi\xi}$ to be symmetric with respect to η-axis. The iteration method used in this study produced values that were non-symmetric and the consequence was an artificial vortex bubble generated by the flow solver at the location where this non-symmetry begins. The problem was solved by assuming the f, and $f_{\xi\xi}$ values for the positive ξ direction to be the same for the negative ξ direction, and by assuming the negative of f_ξ for the positive ξ direction to be the f_ξ values of the negative ξ direction.

As a verification test case, the clean NACA 0012 leading-edge region was placed in a rapid pitch-up maneuver to create a dynamic stall vortex and the results were compared with a previous study, which was done over the entire airfoil by Choudhouri *et al.* [12]. The results of Choudhouri *et al.* [12] are shown in Figure 8. The comparison from the current study is shown in Figure 9 (both plots show the stream function contours). The formation of the primary, secondary and the tertiary vortices are well predicted, as are the general vortex structures. The work by Suito *et al.* [13] considers the entire NACA 0012 airfoil in the same maneuver and produced similar results. It should be noted that care must be taken in the placement of the transition curve between the airfoil and the main parabola. The presence of the transition curve may suppress the vortices and also reduce the rate at which they move downstream. Therefore it is imperative to have a transition curve which merges to the main parabola as far downstream as possible in order to avoid its effects on the upstream flow. As a result of the comparison of the two stream function plots, it can be concluded that the implementation of the leading-edge region of the NACA 0012 airfoil works well and provides reasonable results.

The second verification performed in this study is to assure that the transition curve between the airfoil leading-edge region and the main parabola does not affect the upstream flow, as

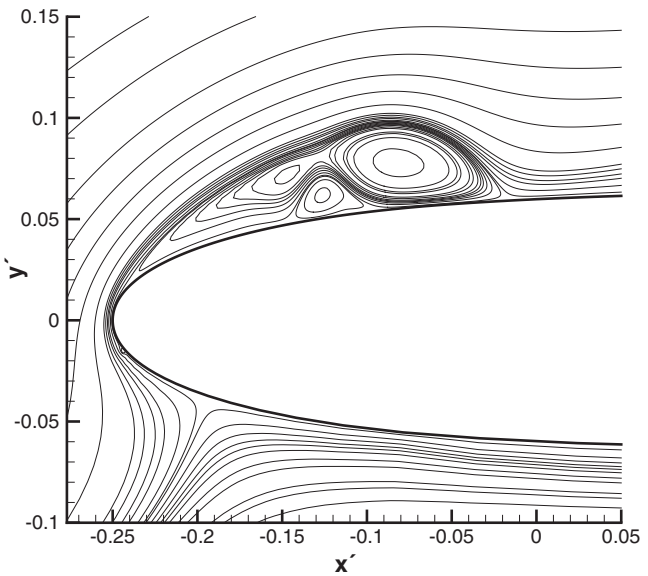

Figure 9. Contours over NACA 0012 in pitch up with grid 1 (481×81).

mentioned above. Different transition curves were used in identical steady, 0° angle-of-attack cases. The results show that the upstream flow remains unaffected provided that there is a sufficient grid resolution and that the transition curve meets the parabola a sufficient distance downstream of the airfoil leading-edge region.

The third verification concerns the use of the Fourier analysis to model the roughness geometry. For this purpose, an analytically defined hump on the parabola surface is modelled by using the Fourier analysis. The formula of the hump in the ξ–η plane is given by

$$f(\xi) = h(\xi - \xi_l)^5(\xi_r - \xi)^5 \tag{13}$$

where h is the user-defined height of the hump, and ξ_l and ξ_r are the left and right boundaries of the hump, respectively. Figure 10 shows the hump geometry as defined by Equation (13) and the regenerated version from the Fourier analysis. As this figure shows, there is a good match between the two shapes.

Over the course of the study, it was found that the number of sine and cosine terms used in the Fourier analysis was a key parameter for the accuracy of the regeneration of the roughness shape. If an insufficient number of terms are used, the regenerated ice shape ($\tilde{f}(\xi)$) may exhibit an excessive amount of smoothing and/or 'wiggles'. If, on the other hand, too many terms are used, the regenerated ice shape becomes extremely sensitive to the changes in the roughness geometry and fluctuates around the original data. Therefore, the correct number of terms is necessary in order to have an accurate modelling of the ice shape geometry. The present study uses an automated iterative subroutine in determining the optimum number of terms to provide a good match with the original roughness data. The number of terms that are used for modelling the selected ice shape in the current study is 40 (i.e. 40 sine and 40 cosine terms).

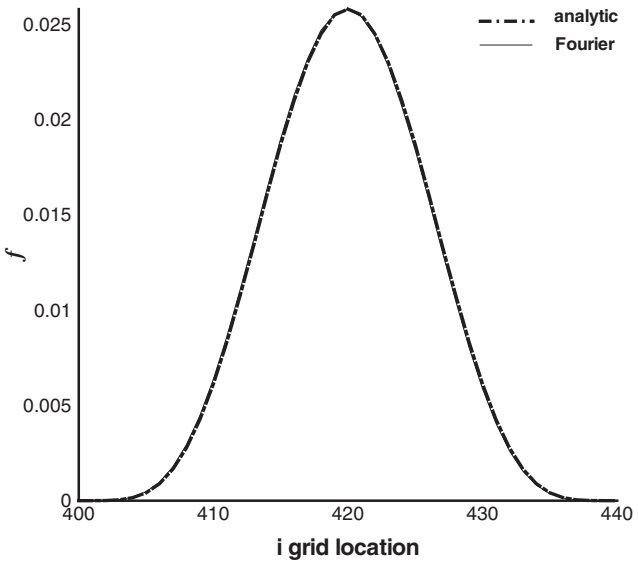

Figure 10. Geometry comparison of a single hump by the analytic formula and the Fourier analysis.

An additional item that affects the accuracy of the regeneration process is the number of control points that are used for the Fourier analysis. If the number of points is not adequate, non-physical oscillations are produced in the regenerated ice shape. Therefore, by parabolic curve fitting, artificial control points are added between every two original control points in the smoothed ice shape in order to increase the accuracy of the regenerated ice shape. Figure 11 shows the comparison of the regenerated ice shape in the physical plane without added control points. In Figure 12, extra control points were added, which produced significant improvement in the accuracy of the roughness modelling as compared to Figure 11. This is particularly true in the roughness around the stagnation point.

The results show that the Fourier analysis performs well in modelling the complex surface geometry, but this accuracy cannot be maintained as far as the derivatives are concerned (see Figure 13). The reason for this is that the Fourier analysis has a 'wavy' nature, which is not consistent with the variation of the surface geometry derivatives in the case of relatively smooth roughness geometries (e.g. single smooth hump). However this deficiency in the calculation of the derivatives can be eliminated by use of central differencing. Since the roughness geometry is fully described by an analytic expression, the first and second derivatives can also be found analytically. However, this study shows that finite central differencing improves the calculation of the derivatives. Figure 13 shows the second derivative for a single hump at various grid locations. This plot compares three different methods for determining the second derivative values: (1) analytic: the hump is described by Equation (13) and exact values for the second derivative are calculated, (2) Fourier: taking the second derivative of the resulting Fourier analysis equation, and (3) central differencing: a central difference stencil is used to calculate the second derivative values using the regenerated roughness data. As Figure 13 shows, the central differencing technique yields better performance with respect to the exact solution.

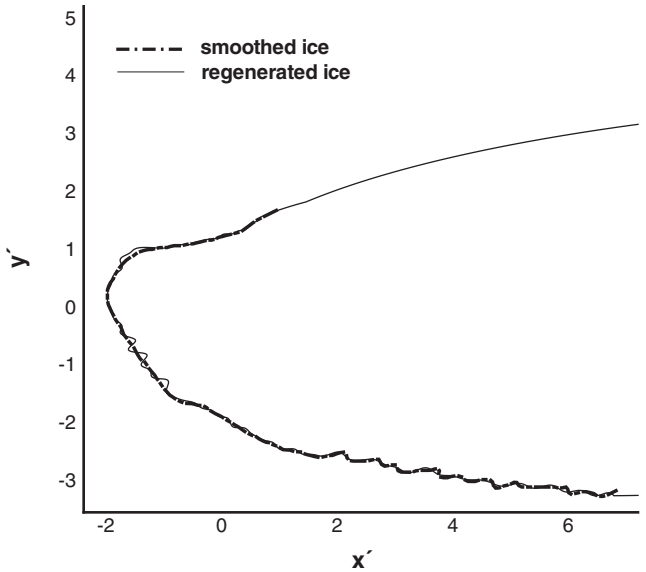

Figure 11. The original smoothed ice shape and the regenerated version, without added cp's.

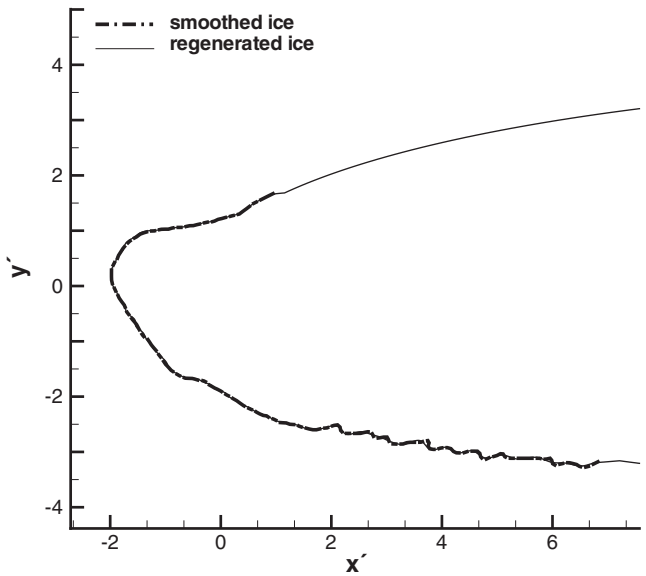

Figure 12. The original smoothed ice shape and the regenerated version, with added cp's.

The impact of the deficiency in modelling the surface derivatives is obvious when comparing the wall vorticity plots over the single hump. In Figure 14, it is seen that the case in which central differencing is used for the derivatives matches very well with the results from the

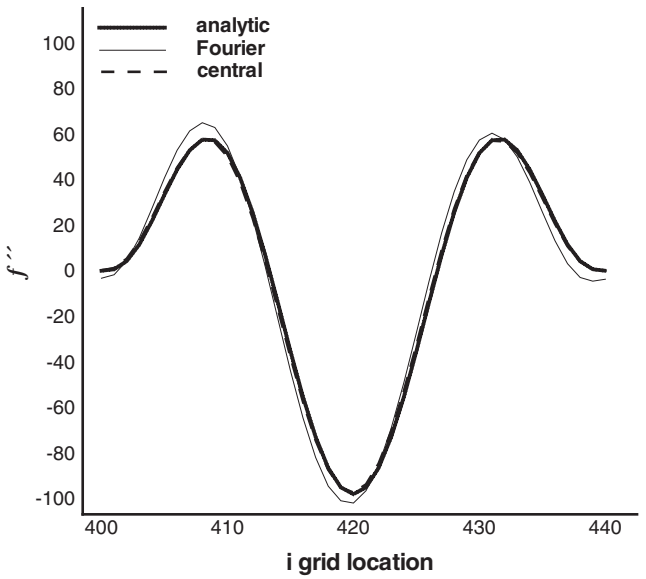

Figure 13. Comparison of three methods to calculate the second derivative.

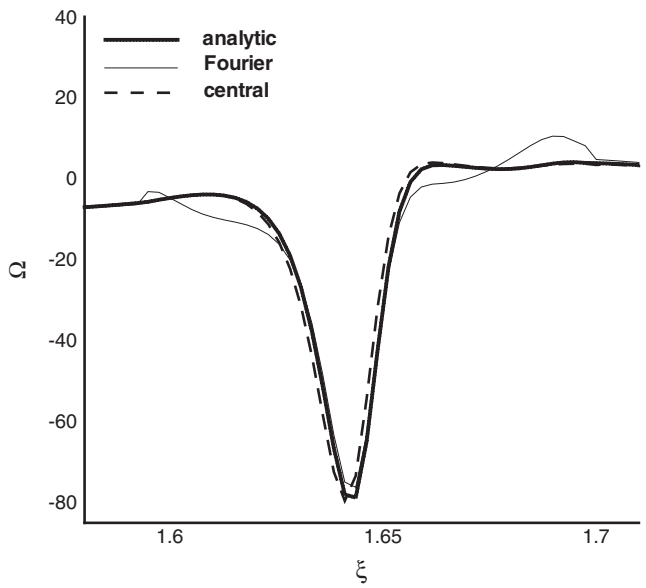

Figure 14. Variation in wall vorticity for different types of derivative analysis (without cp addition).

case in which the geometry is modelled using the analytical formula, whereas the Fourier case produces wiggles.

Having verified the development ideas, these new methods were then used for analysing the flow field past the NACA 0012 leading-edge surface with ice accretion. In the present

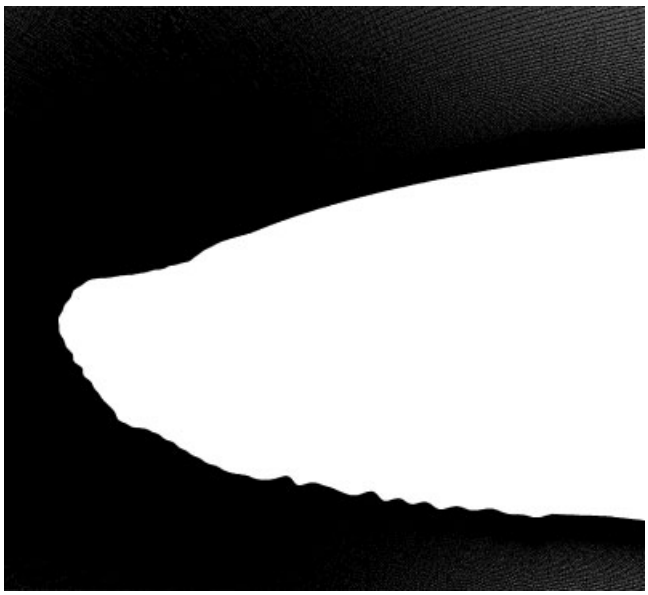

Figure 15. The generated grid over the ice shape.

study, an experimental ice tracing shape, shown in Figure 2, was used for the validation of the Fourier analysis. This is an experimental ice tracing from the NASA Glenn Research Center Image Archive (IRT Image Number: I-1998-000092). The Reynolds number based on the leading-edge radius of curvature was chosen to be 1000. This corresponds to a chord Reynolds number of 0.63×10^5 for the NACA 0012 (see Reference [9] for more details). Based on the above discussion, it was assumed that the addition of extra control points would provide better performance from the Fourier analysis and that the use of central differencing would provide the most accurate simulation for the derivatives.

The automated grid generation scheme outlined in this paper is used for generating the grid over the selected ice shape. An overview of the grid around the ice shape and a zoom-in version are shown in Figures 15 and 16, respectively. As these graphs clearly show, even at a very complex level of roughness, the current scheme can easily generate a fine mesh, which can resolve the flow details. The entire process for generating the grid around the ice shape takes a matter of seconds on a standard computer; this gives a feel for the capability of the current automated grid generation scheme.

In Figures 17 and 18, the wall vorticity plots are shown for flow past the ice shape. The only difference between these figures is that for Figure 17, the Fourier analysis is used for the derivatives whereas for the second figure, central differencing is used for the derivatives. These figures show that, except at the junction points where the ice shape meets the airfoil surface, the two plots look the same. This is a result of the ice shape being inherently a rough and wavy surface, which is consistent with the nature of the Fourier analysis. So, for a complex ice shape such as this, the derivatives at the surface are captured by both the Fourier analysis and central differencing. Figure 19 shows the stream function contours around the NACA 0012 airfoil leading edge with ice accretion. The recirculation regions contained within the roughness of the ice shape can be seen in this figure.

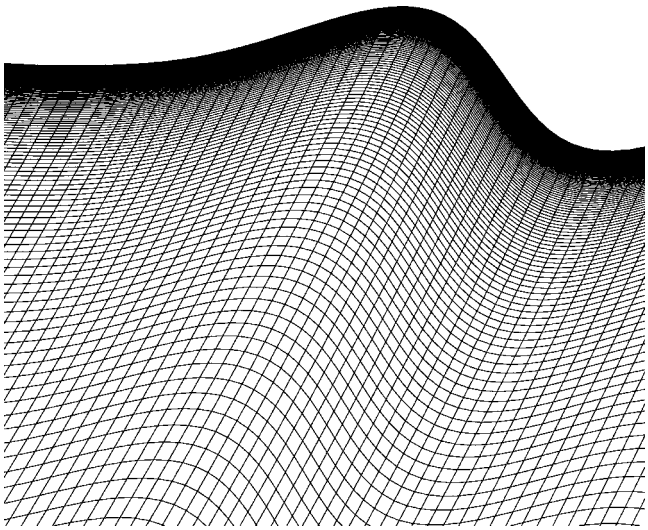

Figure 16. Zoom into the grid over the ice shape.

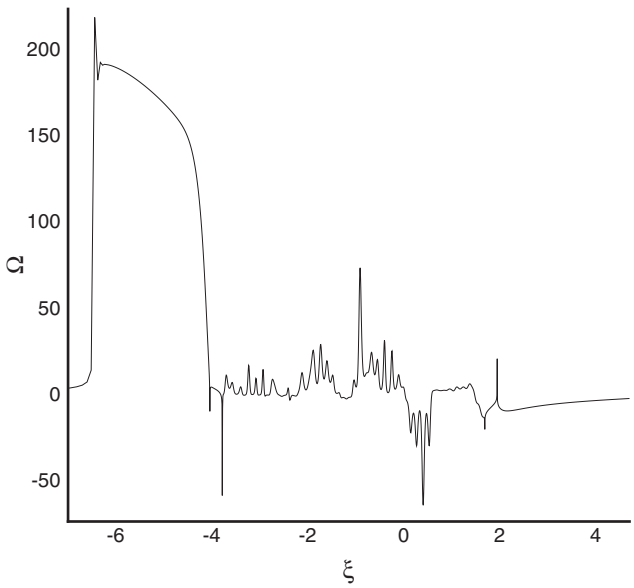

Figure 17. Wall vorticity over the ice shape (Fourier geometry analysis with added cp's and Fourier analysis for the derivatives).

4. CONCLUSIONS

In this study, several geometric modelling enhancements were investigated for implementation into a local-flow Navier–Stokes solver. The enhancements focused on the capability of using

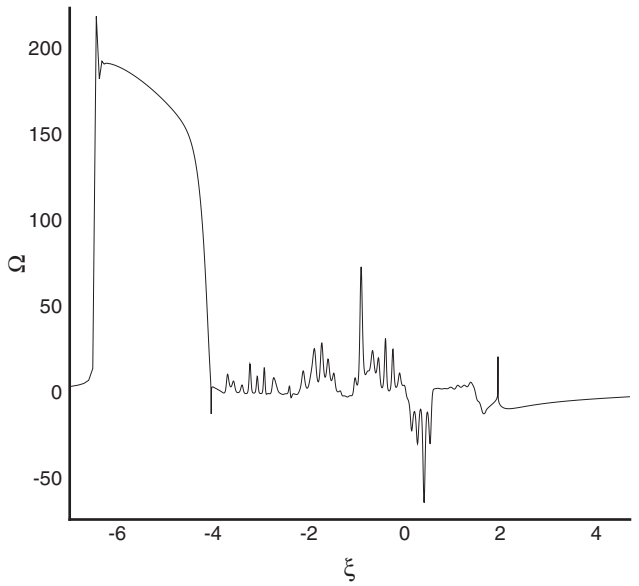

Figure 18. Wall vorticity over the ice shape (Fourier geometry analysis with added cp's and central differencing for the derivatives).

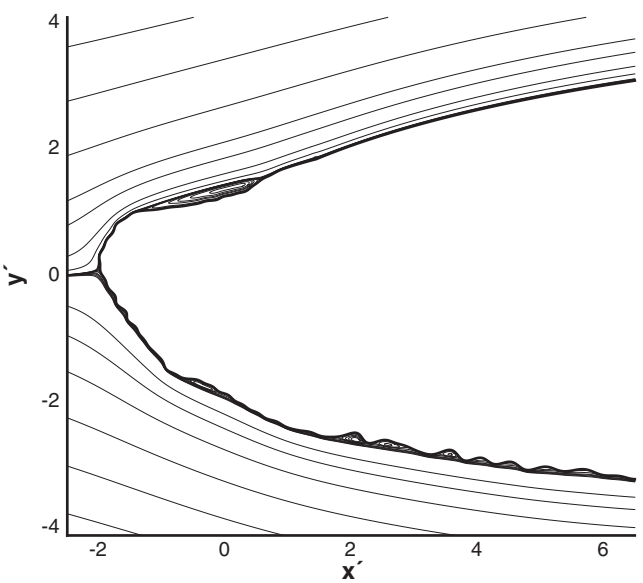

Figure 19. Contours over the ice shape (Fourier geometry analysis with added cp's and central differencing for the derivatives).

actual experimental ice shapes in the flow simulations along with the corresponding airfoil shape. These improved capabilities allow for an automated grid generation process for complex surface roughness and more accurate modelling of the aircraft icing flow field. Although the present study focuses on two-dimensional geometries, the methodologies can be extended to three dimensions and work is currently underway in this direction. The key findings of the current study are summarized below.

1. By studying the flow past a parabola with an analytically well-defined hump, use of the Fourier analysis for the geometry modelling is verified by comparing the results to the analytic case. Use of the Fourier analysis allows actual experimental ice shapes to be incorporated in the flow simulations.
2. It is seen from the same verification study that there are some factors that contribute to the accuracy of the Fourier analysis. These are:
   a. Control point addition to reinforce the modelling. This forces the $\tilde{f}(\xi)$ function to follow the given geometry, instead of wandering in the vicinity of it.
   b. Finding the right number of terms used for the Fourier analysis. This avoids the extreme level of sensitivity of the $\tilde{f}(\xi)$ function against the sudden changes in the geometry.
3. Having regenerated the geometry by the $\tilde{f}(\xi)$ function, use of central differencing for calculating the derivatives on relatively smooth roughness geometries produces better results. For the complex roughness shapes, the Fourier analysis produces results comparable to the central differencing.
4. Use of the leading edge of the airfoil as a perturbation to the parabola leading edge is verified by comparison to a test case in which the entire NACA 0012 airfoil is studied in a rapid pitch-up maneuver.
5. Use of the Fourier analysis and the Prandtl transposition has provided a novel method for automating the grid generation process around a complex ice shape.

REFERENCES

1. Potapczuk MG. Review of NASA Lewis' development plans for computational simulation of aircraft icing. *NASA Technical Memorandum*, No. 208904, January 1999; 21.
2. Vickerman MB, Choo YK, Braun DC, Baez M, Gnepp S. SmaggIce. Surface modelling and grid generation for iced airfoils-phase 1 results. *AIAA paper 2000-0235*, *38th Aerospace Sciences Meeting*, Reno, NV, January 2000.
3. Cebeci T, Besnard E. Prediction of the performance degradation of an aircraft in natural icing conditions. *AIAA paper 94-0487*, *32nd Aerospace Sciences Meeting*, Reno, NV, January 1994.
4. Chung J, Reehorst A, Choo Y, Potapczuk M. Effect of airfoil ice shape smoothing on the aerodynamic performance. *AIAA paper 98-3242*, *34th AIAA/ASME/SAE/ASEE Joint Propulsion Conference*, Cleveland, OH, July 1998.
5. Chung JJ, Addy HE Jr. A numerical evaluation of icing effects on a natural laminar flow airfoil. *AIAA paper 2000-0096*, *38th Aerospace Sciences Meeting*, Reno, NV, January 2000.
6. Chi X, Zhu B, Shih TI-P, Slater JW, Addy HE, Choo YK. Computing aerodynamic performance of a 2d iced airfoil: blocking topology and grid generation. *AIAA paper 2002-0381*, *40th Aerospace Sciences Meeting*, Reno, NV, January 2002.
7. Thompson DS, Soni BK. Automated geometric modelling and grid generation for airfoils with ice accretions. *AIAA paper 2002-0379*, *40th Aerospace Sciences Meeting*, Reno, NV, January 2002.
8. Dunn TA, Loth E. Effects of simulated-spanwise-ice shapes on airfoils: computational investigation. *AIAA paper 99-0093*, *37th Aerospace Sciences Meeting*, Reno, NV, January 1999.
9. Huebsch WW, Rothmayer AP. Effects of surface ice roughness on dynamic stall. *Journal of Aircraft* 2002; **39**(6):945–953.

10. Bhaskaran R, Rothmayer AP. Validation of a Navier–Stokes solver for the leading-edge flow past pitching and oscillating airfoils. *Proceedings of the 6th International Conference on Computational Fluid Dynamics*, Lake Tahoe, NV, September 1995.
11. Davis RT. Numerical solution of the Navier–Stokes equations for symmetric laminar incompressible flow past a parabola. *Journal of Fluid Mechanics* 1972; **51**(3):417–433.
12. Choudhouri PG, Knight DD, Visbal MR. Two-dimensional leading edge separation on a pitching airfoil. *AIAA Journal* 1994; **32**(4):673–681.
13. Suito H, Ishii K, Kuwahara K. Simulation of dynamic stall by multi-directional finite difference method. *AIAA paper 95-2264*, *33rd Aerospace Sciences Meeting*, San Diego, CA, June 1995.

